

# Journal of Biomedical Optics

[SPIEDigitalLibrary.org/jbo](http://SPIEDigitalLibrary.org/jbo)

## **Validation of two-dimensional and three-dimensional measurements of subpleural alveolar size parameters by optical coherence tomography**

Carolin I. Unglert  
William C. Warger, II  
Jeroen Hostens  
Eman Namati  
Reginald Birngruber  
Brett E. Bouma  
Guillermo J. Tearney

# Validation of two-dimensional and three-dimensional measurements of subpleural alveolar size parameters by optical coherence tomography

Carolyn I. Unglert,<sup>a,b</sup> William C. Warger II,<sup>a</sup> Jeroen Hostens,<sup>c</sup> Eman Namati,<sup>a</sup> Reginald Birngruber,<sup>d</sup> Brett E. Bouma,<sup>a,e</sup> and Guillermo J. Tearney<sup>a,e,f</sup>

<sup>a</sup>Harvard Medical School and Massachusetts General Hospital, Wellman Center for Photomedicine, 40 Parkman Street, RSL 160, Boston, Massachusetts 02114

<sup>b</sup>Air Liquide Centre de Recherche Claude-Delorme, Medical Gases Group, 1 Chemin de la Porte des Loges, Les-Loges-en-Josas, France

<sup>c</sup>Bruker microCT, Kartuizersweg 3B, 2550 Kontich, Belgium

<sup>d</sup>University Lübeck, Institute for Biomedical Optics, Peter MonnikWeg 4, 23562 Lübeck, Germany

<sup>e</sup>Harvard-MIT Division of Health Sciences and Technology, 77 Massachusetts Avenue, Cambridge, Massachusetts 02139

<sup>f</sup>Department of Pathology, Massachusetts General Hospital, Boston, Massachusetts 02114

**Abstract.** Optical coherence tomography (OCT) has been increasingly used for imaging pulmonary alveoli. Only a few studies, however, have quantified individual alveolar areas, and the validity of alveolar volumes represented within OCT images has not been shown. To validate quantitative measurements of alveoli from OCT images, we compared the cross-sectional area, perimeter, volume, and surface area of matched subpleural alveoli from micro-computed tomography (micro-CT) and OCT images of fixed air-filled swine samples. The relative change in size between different alveoli was extremely well correlated ( $r > 0.9$ ,  $P < 0.0001$ ), but OCT images underestimated absolute sizes compared to micro-CT by 27% (area), 7% (perimeter), 46% (volume), and 25% (surface area) on average. We hypothesized that the differences resulted from refraction at the tissue–air interfaces and developed a ray-tracing model that approximates the reconstructed alveolar size within OCT images. Using this model and OCT measurements of the refractive index for lung tissue (1.41 for fresh, 1.53 for fixed), we derived equations to obtain absolute size measurements of superellipse and circular alveoli with the use of predictive correction factors. These methods and results should enable the quantification of alveolar sizes from OCT images *in vivo*. © 2012 Society of Photo-Optical Instrumentation Engineers (SPIE). [DOI: 10.1117/1.JBO.17.12.126015]

Keywords: alveolar structure; alveolar volume; ray-tracing; optical coherence tomography.

Paper 12317 received May 20, 2012; revised manuscript received Oct. 1, 2012; accepted for publication Oct. 31, 2012; published online Dec. 12, 2012.

## 1 Introduction

Despite a good understanding of overall lung mechanics, the structure–function relationship at the alveolar level is still insufficiently understood. Quantitative measurements of alveolar sizes and size changes over the physiologic breathing cycle could significantly advance the development of analytical and computational fluid-dynamic models to investigate the mechanisms of gas exchange and aerosol deposition during various ventilation strategies.<sup>1</sup> However, measuring 3- and 4-D alveolar sizes *in vivo* is challenging owing to their small scales and constant motion during respiratory cycles. In a human, for example, alveoli are estimated to be 100–300  $\mu\text{m}$  in diameter with 10- $\mu\text{m}$  walls, and undergo approximately 15 breaths per minute with an overlying cardiac motion of more than 60 beats per minute at rest.

Optical coherence tomography (OCT) has great potential to advance our understanding about pulmonary alveolar structure and function, due to the unique capability to provide three-dimensional (3-D) images at high spatial ( $\sim 10 \mu\text{m}$ ) and temporal ( $> 100$  frames/s) resolution.<sup>2–6</sup> Previous groups have demonstrated OCT visualization of (subpleural) healthy and diseased alveolar morphology in living animal models,<sup>7,8</sup>

and alveolar movement has recently been imaged *ex vivo*<sup>9</sup> and *in situ*.<sup>10</sup> However, artifacts have been reported in the comparison of air-filled and fluid-filled peripheral lung tissue that greatly reduce the imaging depth and create the appearance of double walls.<sup>11,12</sup> It has been hypothesized that these artifacts are caused by the refraction and total internal reflection of light at the tissue–air interfaces and could result in inaccurate representations of alveolar shapes and sizes in OCT images. Thus far, there have been limited quantitative studies on individual alveolar areas,<sup>13,14</sup> and the validity of alveolar volume measures within OCT images has not been shown.

The goal of this study is to investigate the representation of air-filled subpleural alveolar sizes in OCT images to enable quantitative measurements of alveolar cross-sectional area, perimeter, volume, and surface area. We compare OCT images to X-ray microcomputed tomography (micro-CT) images of fixed swine lung to quantify the influence of refraction on alveolar shapes. Micro-CT was used as the gold standard for imaging air-filled peripheral lung tissue because it is subject to minimal refraction artifacts. We confirm the alveolar reconstruction within OCT images with a two-dimensional (2-D) ray-tracing model that calculates the refraction of light at tissue–air interfaces. The refractive indices used in the model were experimentally determined from the analysis of fixed and fresh lung tissue using OCT.<sup>15</sup>

Address all correspondence to: Carolyn I. Unglert, Wellman Center for Photomedicine, 40 Parkman Street, RSL 160, Boston, MA 02114. Tel: 617-724-1359; Fax: 617-726-4103; E-mail: [cunglert@mgh.harvard.edu](mailto:cunglert@mgh.harvard.edu)

In this paper, we show that although refraction and total internal reflection at the tissue-air interfaces significantly influence the visualization of alveolar shapes, the relative alveolar cross-sectional area, perimeter, volume, and surface area can be measured accurately from OCT images without adjustment. Further, we show the potential for absolute size measurements to be obtained with less than 12% average error through the application of correction factors derived from 2-D ray-tracing models.

## 2 Materials and Methods

### 2.1 Sample Preparation

The freshly excised lung from one male Yorkshire swine (~35 kg) was instillation fixed through the airway using a gravity-feed system and dried at 20 cmH<sub>2</sub>O pressure. The fixation solution (modified Heitzman solution) consisted of 10% formaldehyde solution (Fisher Scientific), 10% ethanol (Fisher Scientific), 25% polyethylene glycol 400 (PEG 400, Post Apple Scientific), and 55% laboratory distilled water.<sup>16</sup> Three cylindrical sections were cut (5 mm diameter, 3–5 mm height), each from a different lobe (left upper, right middle, and right lower), such that one circular surface of each sample was delineated by the pleura. All animal experiments were approved and carried out in accordance with the regulations set forth by the Massachusetts General Hospital Subcommittee on Research Animal Care.

### 2.2 Image Acquisition with OCT

A 1310-nm Fourier-domain OCT system referred to as optical frequency domain imaging (OFDI)<sup>2,4</sup> was used to provide 12- $\mu$ m lateral resolution and 8- $\mu$ m axial resolution in air. In this study, fields of view of  $1.5 \times 1.5$  mm ( $512 \times 512$  pixels) in the transverse direction over a ranging depth of 6.6 mm (in air) were acquired with a bench-top galvanometric scanner through the pleural surface of the sample. The acquired voxel size was  $2.9 \times 2.9 \times 6.47$   $\mu$ m in air.

### 2.3 Image Acquisition with Micro-CT

A desktop high-resolution micro-CT system (SkyScan 1172, Kontich, Belgium) with an isotropic voxel size of 2.9  $\mu$ m<sup>3</sup> was used to obtain 3-D cylindrical images with a 3-mm diameter and 0.5-mm height that contained the pleural surface. Each sample was rotated approximately 196 deg at 0.4-deg steps with four projection images averaged per rotation step. Source voltage and current were 40 kV and 250  $\mu$ A, respectively. No external contrast was used.

### 2.4 Segmentation and Measurement of 2- and 3-D Quantitative Alveolar Parameters

To directly compare 2- and 3-D alveolar size parameters, we applied a bicubic interpolation to the OCT images to match the 2.9- $\mu$ m isotropic voxel size of the micro-CT images. Both datasets were then manually reoriented in three dimensions to identify a matching  $1.5 \times 1.5$ -mm field of view between the *en face* planes. Identical alveoli in both data sets were identified by shape and location and then segmented manually in ImageJ.<sup>17</sup> Each alveolar airspace was segmented in the cross-sectional plane along the leading edge of the luminal surface to measure the air inside the alveolus. Openings to a duct or additional alveoli in the axial direction were closed by connecting the incomplete boundary in Fig. 1(c) and 1(d) to limit the analysis to the first layer of alveoli. The closing contour was determined after careful examination of all cross-sectional planes in the 3-D volume of each alveolus to assure a smooth 3-D shape as indicated in Fig. 1(e). Further, individual cross-sections were created and segmented by re-slicing the *en face* data sets along identical line segments. The closing contours were determined analogous to the volume segmentation. An example is shown in Fig. 1(a)–1(d), where Fig. 1(a) and 1(b) show matched *en face* sections from micro-CT and OCT, respectively, as well as the line along which cross-sections Fig. 1(c) and 1(d) were re-sliced. Figure 1(e) shows representative segments for two alveoli across frames (spaced at 30  $\mu$ m) within the micro-CT stack of images,

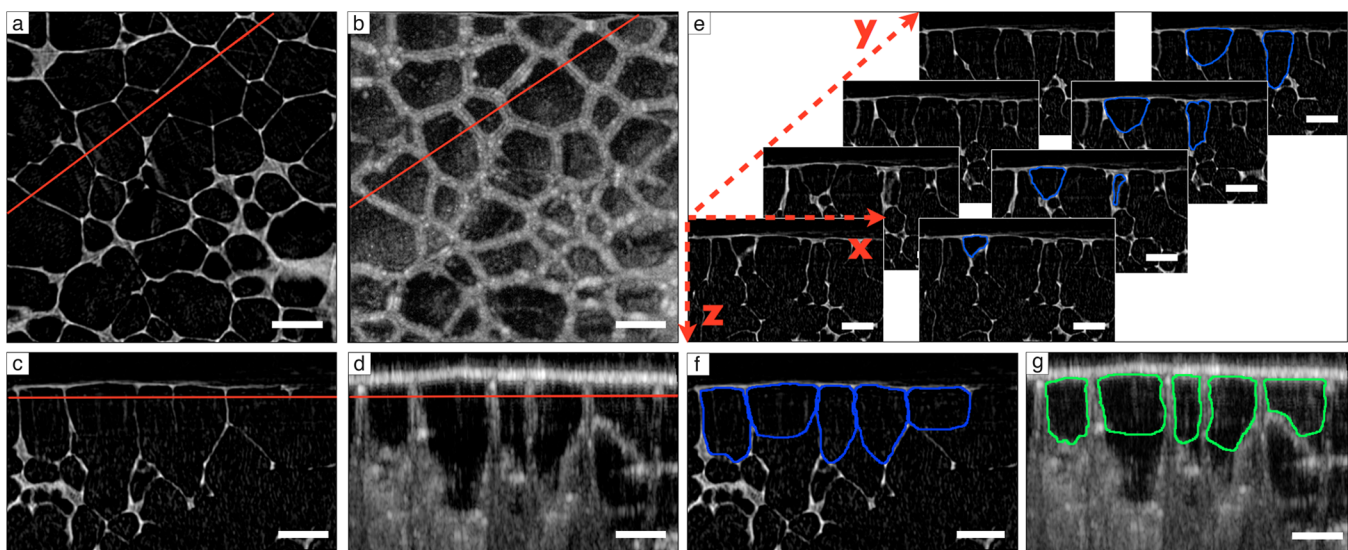


**Fig. 1** Segmentation of alveoli in microcomputed tomography (micro-CT) and optical coherence tomography (OCT) images of fixed swine lung. *En face* micro-CT (a) and OCT (b) images where red line indicates position of axial cross-sectional micro-CT (c) and OCT (d) images. (e) Consecutive frames from micro-CT dataset demonstrate closing of single alveolus with incomplete walls. Comparison of segmentations from micro-CT (f) and OCT (g) axial cross-sections. Scale bars = 200  $\mu$ m.

and Fig. 1(f) and 1(g) show representative segmented alveolar cross-sections from Fig. 1(c) and 1(d), respectively. A total of 29 alveolar cross-sections, at least seven from each lobe, were segmented in both data sets, and the cross-sectional area and respective perimeter were measured in ImageJ. The maximum alveolar height and width were calculated by fitting a bounding rectangle around the segment. For further analysis, the aspect ratio  $f$  of the alveolus was defined as the ratio of height  $h$  over width  $w$ :

$$f = \frac{h}{w}. \quad (1)$$

Further, a total of 19 (at least 5 from each lobe) 3-D, closed alveoli were segmented frame by frame in the cross-sectional plane. The volume of each alveolus was determined by calculating the sum of all cross-sectional areas multiplied by the slice thickness (Simpson's rule). To obtain surface area, we applied a dilation and erosion in the direction orthogonal to the segmentation plane in Matlab to smooth any slight offset between segmented frames, summed the number of pixels along the surface, and multiplied this number by the cross-sectional area of the pixel ( $8.41 \mu\text{m}^2$ ). The alveolar height, width, and depth were calculated in a manner that was analogous to that of the cross-sectional area procedure. The width used to compute the aspect ratio was defined as the arithmetic mean of the width and depth.

## 2.5 Statistical Analyses

Statistical analyses were performed using the software SAS 9.2 and Prism. According to the Shapiro-Wilk test, Gaussian distributions could not be assumed for all size parameters and therefore a nonparametric correlation analysis was performed to correlate the OCT and micro-CT measurements. An absolute  $R$  value  $>0.6$  was assumed to prove a relevant correlation. To estimate how well OCT measurements could be used to conclude absolute values of alveolar size, the slope of the best linear fit between measurements was calculated and compared to the line of identity (slope = 1,  $y$ -intercept = 0). The coefficient of determination  $R^2$  describes how well the line fits the experimental data points. Further, to test whether the slope was significantly different from 1 and the  $y$ -intercept was significantly different from zero, we performed a linear regression analysis of the difference between the two measurements (dependent variable, which was found to approximate a Gaussian

distribution for all size parameters) *versus* the alveolar size as measured in OCT (explanatory variable):

$$(M_{\text{micro-CT}} - M_{\text{OCT}}) = s * M_{\text{OCT}} + t, \quad (2)$$

where  $s$  is the slope of the fit,  $t$  is the intercept, and

$M_{\text{micro-CT}}$

and  $M_{\text{OCT}}$  are the measured values from the micro-CT and OCT images, respectively. A  $P$  value  $<0.05$  was considered statistically significant. Last, the percent measurement error (PE) was also calculated:

$$\text{PE} = \frac{M_{\text{micro-CT}} - M_{\text{OCT}}}{M_{\text{micro-CT}}}. \quad (3)$$

## 2.6 Ray-Tracing Model

We have created a 2-D ray-tracing model in Matlab that calculates the refraction effects (total internal reflection and refraction) based on Snell's law for parallel incident rays on a pre-defined shape to simulate an OCT image. After a qualitative assessment of alveolar shapes that could be observed in the micro-CT images, we chose to approximate the average alveolar cross-section in the model as a superellipse of order 4:

$$\left(\frac{x}{w}\right)^4 + \left(\frac{z}{h}\right)^4 = 1, \quad (4)$$

where  $x$  is the direction parallel to the *en face* plane,  $z$  is parallel to the axial plane,  $h$  is the height of the superellipse, and  $w$  is the width.

Figure 2 illustrates the process of simulating an OCT image. The model calculated the refracted geometric path of each ray through the predefined sample and recorded the distance and refractive index between refraction events [Fig. 2(a)]. Because OCT assumes light travels in a straight A-line, the model translated the recorded geometric path lengths into straight optical path lengths [Fig. 2(b)] to create a simulated OCT image [Fig. 2(d)]. A point spread function (PSF) in the form of an ellipsoidal Gaussian distribution with a width equal to twice the  $12\text{-}\mu\text{m}$  lateral resolution and a height equal to twice the  $8\text{-}\mu\text{m}$  axial resolution of the OCT system was applied with a 2-D convolution to make the borders of the alveoli in Figs. 2(d), 7(e), 9(b),

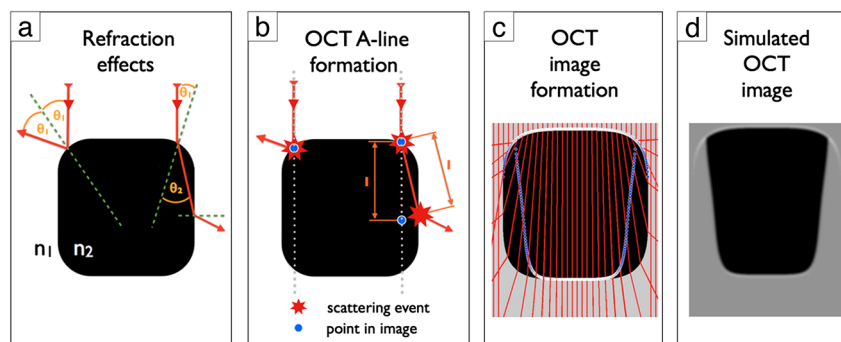


**Fig. 2** Simulation of OCT image based on ray-tracing model. (a) Light rays incident upon interface with refractive index ratio  $n_1/n_2$  will refract or totally internally reflect. (b) OCT collects backscattered and reflected light from these interfaces but assumes the light has traveled along straight A-line. (c) Ray-tracing model calculates path of parallel rays through alveolus and records traversed refractive indices  $n_1$  and  $n_2$  to reconstruct simulated OCT image (d).

and 9(c) more apparent to the reader. The PSF convolution was not performed at any point during the quantitative analyses.

Quantitative size parameters between the alveolus within the original and the simulated image were compared. The difference in cross-sectional area was calculated by summing the total number of pixels representing air within a single image. The perimeter was calculated by summing the lengths of all of the hypotenuses between the ends of subsequent rows to create a contour of the discretized shape. We further computed the volume by assuming each row was rotationally symmetric and summing the circular cross-sections for each row through the height of the superellipse. The surface area was calculated according to the first Guldinus theorem:

$$SA = 2\pi * L * R_{\text{grav}}, \quad (5)$$

where  $L$  is the arc length of curve generating the rotationally symmetric object and  $R_{\text{grav}}$  is the center of gravity of  $L$  with respect to the symmetrical axis.

Last, to establish potential correction factors, we modeled the error analogous to Eq. (3) for a range of aspect ratios ( $f = 0.4$ – $2$  with an increment of  $0.1$ ) and refractive index ratios ( $n_{\text{ratio}} = n_{\text{tissue}}/n_{\text{air}} = 1.04$ – $1.61$  with an increment of  $0.01$ ). Using Matlab's surface-fitting toolbox, we then deduced separate polynomial equations from the discrete modeling results to compute the correction factor as a function of  $f$  and  $n$  in the tested range for all size parameters. We chose the lowest orders of the polynomial that provided a fit with residuals less than 5% error. The goodness of fit was characterized by  $R^2 > 0.99$ , with the exception of the perimeter, where  $R^2 > 0.91$ .

## 2.7 Refractive Index Measurement

Representative values of the mean refractive index of mammalian lung tissue were determined using OCT.<sup>15</sup> Fresh and fixed swine lung tissue were ground in a freezer mill (SPEX 6770) to

create bulk lung tissue paste for each tissue type, which was placed on a planar reflective surface and warmed to  $37^\circ\text{C}$ . A total of 33 measurements were recorded from each sample (three measurements from 11 separate images) to provide a group refractive index of  $1.41 \pm 0.003$  (mean  $\pm$  SE) for fresh and  $1.53 \pm 0.003$  for fixed swine lung tissue illuminated at  $1310 \pm 55$  nm.

## 3 Results

### 3.1 OCT vs. Micro-CT Comparison of Segmented Alveolar Sizes

In this study, we compared 2- and 3-D sizes of identical pulmonary alveoli as represented in OCT images versus micro-CT images. A correlation analysis showed that OCT provides highly representative measures of relative alveolar cross-sectional area ( $R = 0.95$ ,  $P < 0.001$ ), perimeter ( $R = 0.93$ ,  $P < 0.001$ ), volume ( $R = 0.91$ ,  $P < 0.001$ ), and surface area ( $R = 0.93$ ,  $P < 0.001$ ). However, when OCT measurements were plotted as a function of micro-CT measurements, the slope of the linear fit was smaller than 1 for all size parameters, equal to 0.78 for cross-sectional area, 0.88 for perimeter, 0.62 for volume, and 0.78 for surface area, indicating that OCT systematically underestimated the absolute alveolar sizes compared to micro-CT. Consequently, OCT did not allow the prediction of absolute alveolar sizes as measured by micro-CT. This is visualized in Fig. 3 and confirmed by a linear regression analysis showing that the slope  $s$  in Fig. 3 was significantly different from 1, with the y-intercept  $t$  significantly different from 0 for cross-sectional area ( $P_s = 0.006$ ,  $P_t = 0.044$ ,  $R^2 = 0.25$ ) and volume ( $P_s = 0.003$ ,  $P_t = 0.016$ ,  $R^2 = 0.42$ ). The relationship was not significant for perimeter ( $P_s = 0.003$ ,  $P_t = 0.477$ ,  $R^2 = 0.01$ ) or surface area ( $P_s = 0.27$ ,  $P_t = 0.08$ ,  $R^2 = 0.07$ ).

The intra-data variability as a function of alveolar size can be observed in Fig. 4 from the mean  $\pm$  SD of the percent

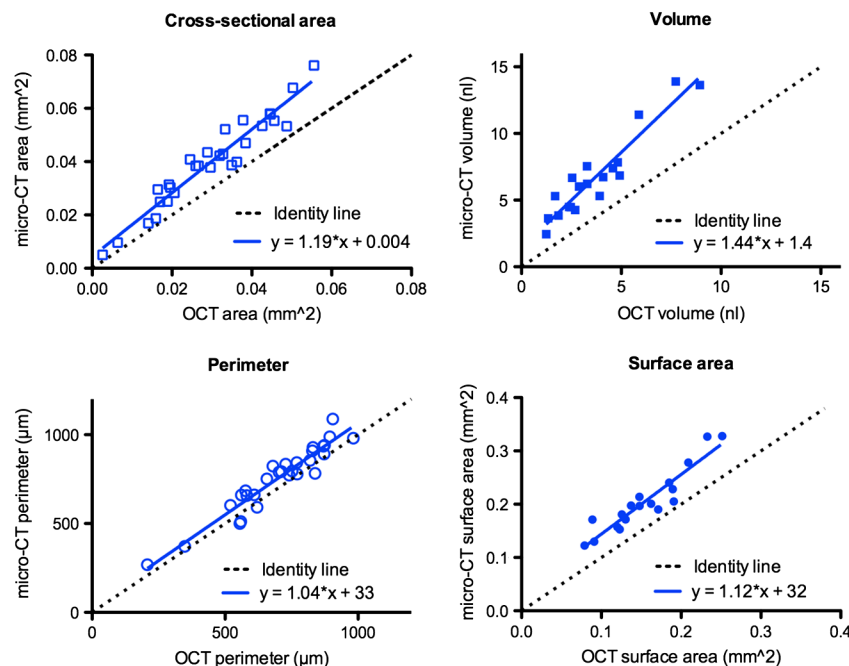


**Fig. 3** Comparison of alveolar size measurements (cross-sectional area, volume, perimeter, and surface area) obtained from micro-CT images (y-axis) and OCT images (x-axis). Linear fit ( $R^2 \geq 0.88$ ) shown for all parameters compares to identity line (dotted black line), which indicates perfect agreement.

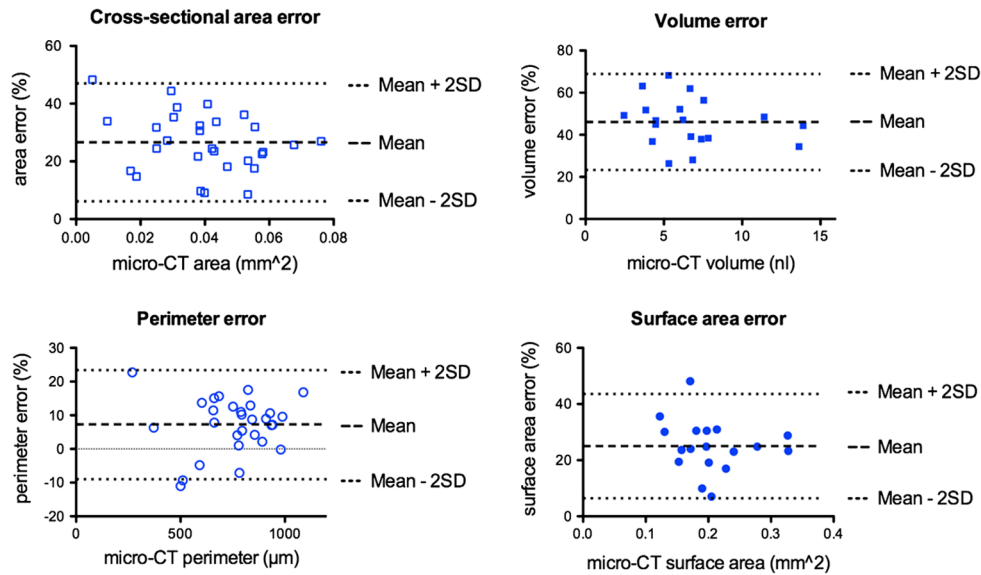


**Fig. 4** OCT measurement error for alveolar size measurements (cross-sectional area, volume, perimeter, and surface area) as a function of micro-CT alveolar size.

error for area ( $27\% \pm 10\%$ ), perimeter ( $7\% \pm 8\%$ ), volume ( $46\% \pm 11\%$ ), and surface area ( $25\% \pm 9\%$ ).<sup>18</sup> The difference between the OCT and micro-CT measurements could not be correlated significantly to the respective alveolar sizes, but the data suggest a statistically significant increase in error with increasing aspect ratio of the alveolus [from Eq. (1)] for area ( $P = 0.008$ ,  $R^2 = 0.234$ ), volume ( $P = 0.0004$ ,  $R^2 = 0.53$ ), and surface area ( $P = 0.029$ ,  $R^2 = 0.27$ ). A plot of the percent error versus  $f_{CT}$  is shown in Fig. 5 in the following section,

where the experimental results are compared to the modeling. The relationship for the perimeter was not significant but the plot is provided for completeness.

### 3.2 Modeled Influence of Refraction

The ray-trace modeling results predict a 22% underestimation for cross-sectional area and 5% underestimation for the perimeter of a superellipse with equal width and height and a

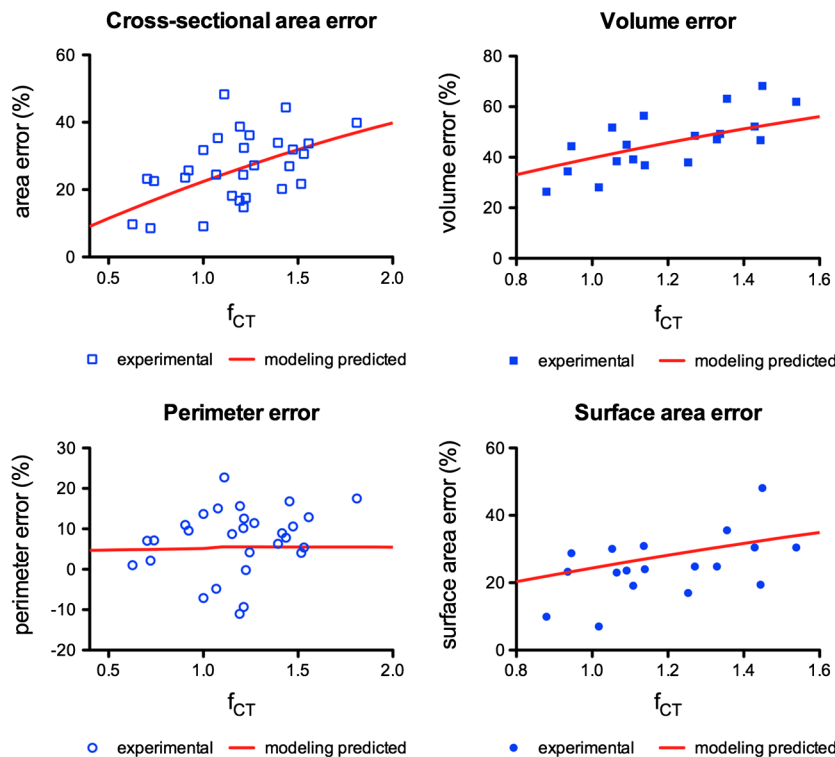


**Fig. 5** Qualitative comparison of experimental OCT measurement error (blue datapoints) versus predicted modeling results (red line) as a function of alveolar aspect ratio for cross-sectional area, volume, perimeter, and surface area. Predicted result (red line) calculated from Eq. (7), polynomial coefficients in Table 2, and  $n_{ratio} = 1.53$ .

**Table 1** Polynomial coefficients ( $P_{fn}$ ) to be inserted into Eq. 6 to compute correction factors for alveolar superellipse measurements with  $n_{\text{ratio}} = 1.04\text{--}1.61$ .

Coefficients	$P_{00}$	$P_{10}$	$P_{01}$	$P_{20}$	$P_{11}$	$P_{02}$
Cross-section	-93.76	-0.9008	128.9	-3.012	17.88	-44.63
Perimeter ( $f \leq 1$ )	2.749	0.7287	1.083	0	0	0
Perimeter ( $f > 1$ )	3.707	-0.0683	1.258	0	0	0
Volume	-179.9	15.77	242.9	-7.272	19.86	-81.55
Surface area	-105.7	-0.09633	147.2	-3.317	17.20	-50.42

refractive index ratio between the tissue and alveolar filling  $n_{\text{ratio}} = 1.53$ . The model further predicts an underestimation of 40% for the volume and 25% underestimation for the surface area of a circularly symmetric superellipsoid with equal width and height. The modeling predicted error is shown to depend on both  $n_{\text{ratio}}$  and the aspect ratio of the alveolus in Eq. (1), such that alveoli with an aspect ratio below 1 (short and wide) will be visualized with less error. Eq. (6) was derived to compute the error:

$$E_{\text{pred}} = P_{00} + P_{10} * f + P_{01} * n_{\text{ratio}} + P_{20} * f^2 + P_{11} * f * n_{\text{ratio}} + P_{02} * n_{\text{ratio}}^2 \quad (6)$$

for the cross-sectional area, perimeter, volume, and surface area for an alveolar superellipse as a function of  $f$  and  $n_{\text{ratio}}$  with the polynomial coefficients from Table 1.

Figure 5 shows the experimentally obtained errors as a function of the aspect ratio and compares the results to the model for a refractive index ratio of 1.53. The mean  $f_{\text{CT}}$  of the alveoli segmented in this study was 1.2, corresponding to modeling

predicted percent errors of 26% for cross-sectional area, 5% for perimeter, 46% for volume, and 28% for surface area. For comparison, the experimentally obtained mean errors were 27% (area), 7% (perimeter), 46% (volume), and 25% (surface area).

### 3.3 Correction of Alveolar Size Measurements

To test whether the modeling predicted error ( $E_{\text{pred}}$ ) from section 3.2 could be used as a correction factor to compute absolute measures ( $m_{\text{pred}}$ ) of alveolar size from the originally segmented OCT data, we determined  $f_{\text{OCT}}$  of each alveolus from the OCT images and scaled the originally measured sizes ( $m_{\text{OCT}}$ ):

$$m_{\text{pred}} = \frac{m_{\text{OCT}}}{1 - E_{\text{pred}}} \quad (7)$$

The resulting mean error between the corrected OCT measurements and the original micro-CT measurements was -1% for cross-sectional area, 2% for perimeter, -11% for volume, and -9% for surface area. Figure 6 illustrates the comparison

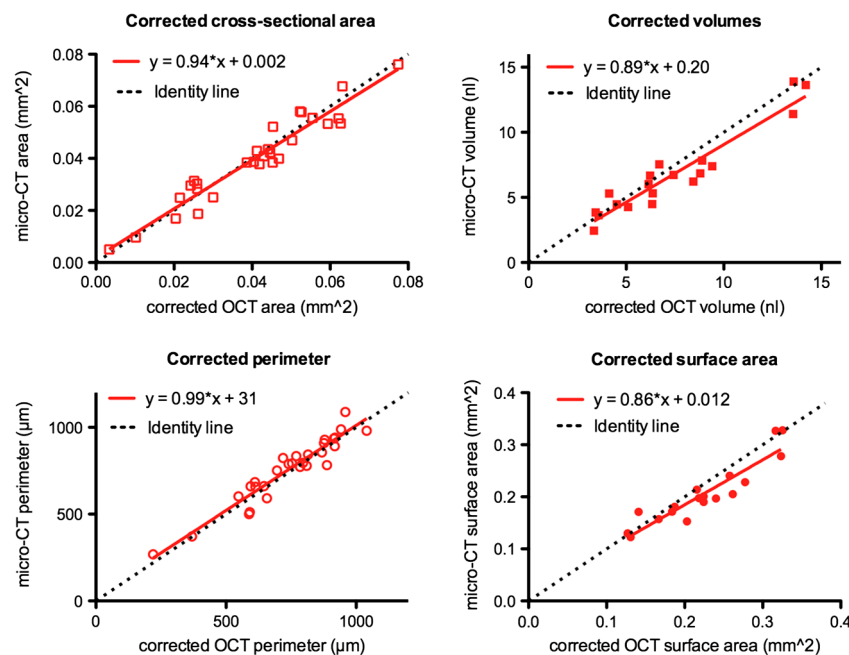


**Fig. 6** Comparison of alveolar size measurements (cross-sectional area, volume, perimeter, and surface area) obtained from micro-CT images (y-axis) and corrected OCT measurements according to modeling predicted error (x-axis). A linear fit ( $R \geq 0.85$ ) shown for all parameters compares to identity line (dotted black line), which indicates perfect agreement.

of alveolar sizes as measured with micro-CT *versus* the predicted values and compares a linear fit of the data to the identity line analogous to Fig. 3. Neither slopes nor intercepts of the corrected values could be shown to be statistically significantly different from 1 or 0, respectively.

## 4 Discussion

### 4.1 Summary

In this study, we investigated the effect of refraction and total internal reflection on the representation of subpleural alveolar cross-sectional area, perimeter, volume, and surface area within OCT images. OCT and micro-CT images of the same fixed swine lung samples were compared, where micro-CT was considered a gold standard for visualization of the true alveolar size. Under this assumption, we showed that OCT provides alveolar size measurements that are highly correlated to measurements from micro-CT. The absolute alveolar size parameters, however, were significantly underestimated, independent of alveolar size. Second, we presented the results of a ray-tracing model that calculated the expected error of OCT size measurements resulting from refraction artifacts. The predicted error from the model corresponded very well to the experimentally determined mean error, and both showed an increasing error with increasing aspect ratio, indicating that refraction and total internal reflection at the tissue-air interfaces are the primary reasons for the underrepresentation of alveolar size in OCT images. Further, the modeling results allowed us to derive scaling factors that were used to correct the initial OCT measurements and successfully approximate the absolute average micro-CT values.

### 4.2 Differences between Fresh *In Vivo* and Fixed Subpleural Alveolar Tissue

This study was conducted as a crucial step toward validating alveolar size measurements made from OCT images of subpleural alveoli *in vivo*. We chose to compare OCT measurements against micro-CT on small samples of fixed swine lung to image the same field of view with both technologies at the same inflation state and with similar spatial resolution. Adequate resolution could not have been obtained in micro-CT images of a whole swine lung, since the resolution of micro-CT depends on the transmission of the X-rays through the sample to capture the absorption profile, whereas OCT collects the back-scattered light. Further, the samples could be easily transported between imaging technologies without creating morphologic changes to the sample.

We expect three main differences between fixed tissue and *in vivo* mammalian subpleural alveoli. First, the lower refractive index of the living tissue, and therefore the lower refractive index difference at the tissue-air interfaces, will reduce the refraction artifacts within the OCT measurements. According to our measurements of the group refractive indices of fixed and fresh healthy lung parenchyma, the refractive index would decrease from 1.53 to 1.41. Therefore, we expect conclusions drawn from fixed tissue to remain proportional when transitioning to fresh tissue, and this difference can be modeled for absolute measurements. It is important to note that in diseased lungs, both the refractive index of the lung tissue as well as the refractive index of the alveolar space could be altered. For example, the alveoli could be fluid filled in pulmonary edema or the

alveolar tissue could contain an excess of collagen in interstitial fibrosis.

Second, the *in vivo* alveolar size of a specific alveolus is expected to change dynamically during inflation and deflation of the lung. In contrast, the alveoli in this study were representative of a single inflation pressure (20 cmH<sub>2</sub>O) and were fixed outside of the body where they were not subject to the effects of the chest wall. Both our experimental and modeling results indicate that the percent measurement error caused by refraction artifacts was independent of alveolar size. Therefore, we believe the results from different-sized alveoli at a single inflation state are representative of the change in alveolar size *in vivo*.

Last, the alveolar shape could change dynamically during the breathing cycle. For example, the upper surface of subpleural alveoli could flatten out as overall lung volume increases. From our modeling results, we believe that the error is significantly dependent on the alveolar shape. More specifically, the error increases with increasing curvature of the upper surface of the alveolus and increasing aspect ratio. A circular cross-section of air-filled fresh tissue ( $n_{\text{ratio}} = 1.41$ ), for example, would have an error of 29.3%, which corresponds to the error expected for a superellipse of  $f = 1.52$ , and compares to 20.6% error for a superellipse with equal width and height. This alveolar shape dependence of the measurement error could be the primary cause for the spread in the experimentally determined error values.

### 4.3 *In Vivo* Measurements of Relative Subpleural Alveolar Size

We were able to show excellent correlation for relative measures of alveolar cross-sectional area, perimeter, volume, and surface area between OCT and micro-CT images. This leads us to conclude that OCT could be used to answer important questions about alveolar structure and function without any correction. However, for exact results and depending on the research question, we recommend an assessment of the alveolar shape change. For example, OCT could potentially be employed to quantify the dynamic percent volume change of specific alveoli during the breathing cycle. In this case, the use of relative measurements would only provide the same results as using corrected measurements if alveolar expansion and contraction were isotropic. Similarly, to quantify relative regional differences or compare clusters of alveoli in healthy and diseased lungs, the shape characteristics between the clusters of alveoli should be similar. Where the necessary assumptions about alveolar shape cannot be made, the measured sizes should be corrected to analyze absolute sizes.

In addition to being based on the analysis of fixed tissue, our results were obtained evaluating a single lung from a single species, swine. Because we were able to approximately explain and validate our experimental results *via* a model, however, we expect our conclusions to remain valid for all mammalian species where single subpleural alveoli can be identified in OCT images.

### 4.4 Correction of OCT Measures of Subpleural Alveolar Size

Some studies may require evaluating absolute values of alveolar size or a quantification of the change in percent error. Computational fluid dynamic (CFD) models of aerosol deposition in the alveolar region, for example, could profit from exact data



about the direction and magnitude of alveolar expansion and contraction.<sup>1</sup>

In this study, we provided correction factors as a function of the refractive index of the tissue and the alveolar aspect ratio to account for the underrepresentation of alveolar sizes in OCT due to refraction effects. These factors are based on our 2-D ray-trace model of a superellipse-shaped cross-section. Further, we tested these factors for correcting the previously discussed OCT measurements of fixed swine lung samples and could reduce the absolute mean error compared to micro-CT below 12% for all size parameters. The wavelength dependence of the refractive index was not considered in the analysis because the difference in refractive index over the 100-nm bandwidth of our light source was estimated to be approximately 0.1% based on the 0.2% change in index for water between 1.2 and 1.4  $\mu\text{m}$ .<sup>19</sup> The measured refractive indices also correspond well to previously published results. The refractive index of fresh lung tissue was measured to be 1.38 at a wavelength of 632.8 nm,<sup>20</sup> and important constituents of lung tissue have been shown to have indices of 1.33–1.35 (interstitial liquid), 1.39 (nuclei), 1.41 (connective tissue fibers), and 1.61–1.66 (red blood cells) in the visible wavelength range.<sup>21</sup> The higher refractive index of the fixed tissue could be due to the fixation solution containing PEG 400 (refractive index of 1.47) and the subsequent drying that reduced the water content of the tissue.

Based on the assumptions of the ray-trace model, these correction factors are recommended where alveolar shapes resemble superellipse cross-sections. They were computed for a range of tissue refractive index ratios between 1.04 and 1.61 and require a measure of the aspect ratio for each alveolus. Further, we expect the scaling factors to more efficiently correct 2-D measurements compared to 3-D, as discussed in more detail in the following subsections. It is also interesting to note that the correction factors for the perimeter are primarily given for completeness. In the evaluated index and aspect ratio ranges, the modeling predicted perimeter error did not exceed 6%.

#### 4.4.1 Alveolar shape

The superellipse shape was chosen because it seemed to provide the most accurate representation of the general subpleural alveolar shape within the micro-CT images. It is important to note, however, that the superellipse was a large simplification for the individual cross-sections. The upper surface of the alveoli within the micro-CT images ranged from almost completely rounded to completely flat, and the walls could be vertical or inclined. Cross-sectional shapes of the same alveolus also varied depending on the location and angle at which they were evaluated. Further, the correction factors were based on fully closed alveoli. In reality, none of the fixed alveoli are completely closed in three dimensions, and even single 2-D cross-sections must often be closed manually during segmentation to compute cross-sectional area. The spread of percent error in corrected measurements for a given size or aspect ratio could in part be caused by the discrepancy between the real and modeled shape.

*In vivo* alveolar shapes could potentially differ more significantly from the superellipse, and the correction factors would have to be re-evaluated accordingly. For a circular cross-section, for example, correction factors could be calculated according to Eq. (8) and Table 2. Although any specific shape could in principle be modeled to obtain exact correction factors, alveolar

**Table 2** Polynomial coefficients ( $P_n$ ) to be inserted into Eq. 8 for circular alveoli with  $n_{\text{ratio}} = 1.00\text{--}1.61$  to calculate correction factors for alveolar size measurements.

Coefficients	$P_0$	$P_1$	$P_2$
Cross-section	-136.4	184.2	-47.29
Perimeter	-41.86	58.53	-16.26
Volume	-275.8	389.7	-112.4
Surface area	-170.8	236.5	-64.55

shapes can be evaluated only under the influence of refraction artifacts within *in-vivo* OCT images due to the lack of comparable micro-CT data. However, refraction artifacts are expected to be less severe *in vivo* owing to the smaller refractive index ratio.

$$E_{\text{pred}} = P_0 + P_1 * n_{\text{ratio}} + P_2 * n_{\text{ratio}}^2. \quad (8)$$

#### 4.4.2 Aspect ratio

Similar to the general appearance of the alveolar shape, the aspect ratio evaluated within *in vivo* OCT images is also subject to refraction artifacts. For the alveoli segmented in this study, we found that the OCT aspect ratio was closely related to the micro-CT aspect ratio ( $P < 0.0001$ ,  $R^2 = 0.69$  for area and perimeter,  $P < 0.0001$ ,  $R^2 = 0.80$  for volume and surface area). Using the micro-CT aspect ratio instead of the OCT aspect ratio for the calculation of the correction factor would have only slightly improved the analysis of the scaled measures compared to micro-CT: 1% mean error (compared to -2%) for cross-sectional area, 2% mean error (compared to 2%) for perimeter, 2% mean error (compared to -11%) for volume, and -4% mean error (compared to -9%) for surface area. It therefore seems reasonable to correct OCT measurements of alveolar size based on the aspect ratio visualized in the same images.

#### 4.4.3 2-D versus 3-D alveolar sizes

Although the absolute mean error for all sizes was reduced to less than 12%, the correction factors performed better for the 2-D cross-sectional area and perimeter than for the 3-D volume and surface area. This could have been caused by two approximations that were made for the 3-D case. First, the simulated OCT image was directly modeled for the 2-D case and the 3-D error was calculated assuming the 2-D result was circularly symmetric throughout the height of the alveolus. This stronger discrepancy between the real and modeled shape for the 3-D case could explain the larger difference between the actual and the modeling predicted measurement error. Second, to calculate the appropriate correction factor, the 3-D aspect ratio was reduced to two dimensions. The alveolar width of the 3-D aspect ratio was defined as the mean of the alveolar width and depth as measured from the two transverse planes. To determine the exact correction factor per alveolus, each specific alveolar shape should be modeled in three dimensions.

#### 4.4.4 Fluid-filled alveoli

It is interesting to note that some studies have chosen to minimize refraction artifacts by filling the alveolus with fluid, such as saline, ethanol, or perfluorodecalin.<sup>11,22,23</sup> Our modeling results confirm the efficacy of this approach. According to Eq. (6) and Table 1, assuming a superellipse shape with an aspect ratio of 1.2, a tissue refractive index of 1.41 and a fluid-filled refractive index of 1.30 ( $n_{\text{ratio}} = 1.085$ ), the expected error is 11% for cross-sectional area, 5% for perimeter, 22% for volume, and 12% for surface area. Compared to the air-filled case, the error in alveolar size measures from fluid-filled alveoli would be more than halved.

#### 4.5 Alternative Segmentation to Obtain Absolute Alveolar Sizes

We have shown that OCT measurements of alveolar size can be corrected to yield absolute values using modeling predictive factors. For exact results, however, the correction factors should be determined by modeling the specific 3-D shape of each alveolus. It could therefore be advantageous to obtain correct absolute alveolar sizes directly through segmentation that accounts for the primary refraction artifacts, such as the appearance of two walls per alveolus.<sup>11</sup> We also frequently observed triple walls between adjacent alveoli in our OCT images and confirmed the additional walls as artifacts through the comparison of the same alveolar wall in OCT and micro-CT images [Fig. 7(a)–7(d)] and *via* ray-trace modeling of two adjacent airspaces [Fig. 7(e)]. We further quantitatively confirmed the hypothesis that the outer two of three walls would be artifacts in OCT images and could be excluded from segmentation. Therefore, we re-segmented the original alveoli in the OCT images by tracing the boundary along the central of three apparent alveolar walls and compared the newly segmented alveolar sizes to those measured in micro-CT images. Alveolar cross-sections were re-segmented within the cross-sectional plane and alveolar volumes within the *en-face* plane. Where no three clear walls could be identified, the boundary was traced near the

center of the wall between alveoli. Fig. 7(f) and 7(g) illustrate the alternative segmentation methods. Figure 8 shows the micro-CT sizes over the newly segmented OCT values and compares the linear fit to the experimental data points to the line of identity similar to Fig. 3.

Mean errors for this alternative segmentation technique in cross-sectional area and perimeter were reduced from 27% and 7% (original segmentation method) to 7% and 0%, respectively. Mean errors in volume and surface area were reduced from 46% and 25% to 5% and -6%, respectively. Statistically, the slope of the linear fit remained significantly different from 1 for cross-sectional area and surface area, but could not be shown to be different from 1 for volume. The *y*-intercept was statistically different from 0 only for surface area. The nonparametric correlations of size measurements between the techniques remained equally high for cross-sections ( $R = 0.96$ ,  $P < 0.0001$ ), perimeter ( $R = 0.91$ ,  $P < 0.0001$ ), volumes ( $R = 0.93$ ,  $P < 0.0001$ ), and surface area ( $R = 0.91$ ,  $P < 0.0001$ ).

As expected, this alternative segmentation could be advantageous over a correction of sizes according to the modeling results for 3-D measurements, since the exact 3-D shape of each individual alveolus as well as the 3-D effect of refraction are considered. However, this approach requires that the refraction effects result in distinguishable real and artificial alveolar walls. Although we have frequently observed these multiple walls in fixed excised lungs, it is unclear under which circumstances the effect would be seen *in vivo* and whether it could be misinterpreted in the case of de-recruited alveoli in between recruited alveoli. We therefore recommend the segmentation over the correction approach where absolute alveolar volumes and surface area must be determined in images showing triple walls.

#### 4.6 Applicability to Non-subpleural Alveoli

It is important to emphasize that we limited our analysis to the first layer of alveoli beneath the pleura. As previously described,<sup>11</sup> the imaging depth in air-filled alveolar tissue is significantly compromised compared to fluid-filled alveoli. Fig. 9

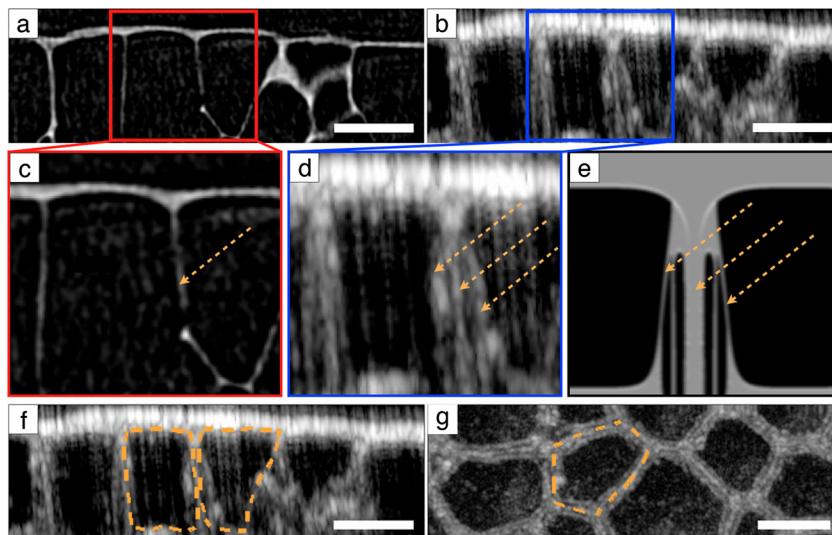


**Fig. 7** Illustration of triple-wall artifacts and an alternative segmentation method. A single alveolar wall (dashed arrow) in micro-CT (a, c) image appears as three separate walls (dashed arrows) in the corresponding OCT (d, e) image. (e) Ray-trace simulation of two adjacent alveoli confirms outer two of three walls can result from refraction artifacts. Alveoli were alternatively segmented at middle of alveolar wall in axial cross-sectional (f) and *en-face* (g) planes.

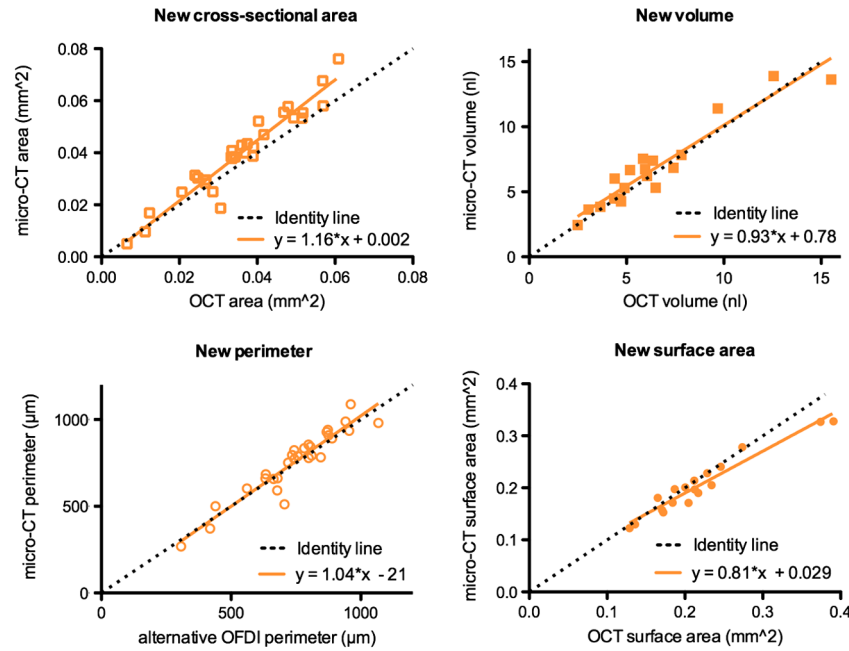


**Fig. 8** Comparison of alveolar size measurements (cross-sectional area, volume, perimeter, and surface area) obtained from micro-CT images (y-axis) and alternatively segmented OCT images (x-axis). A linear fit ( $R^2 \geq 0.88$ ) shown for all parameters compares to identity line (dotted black line), which indicates perfect agreement.

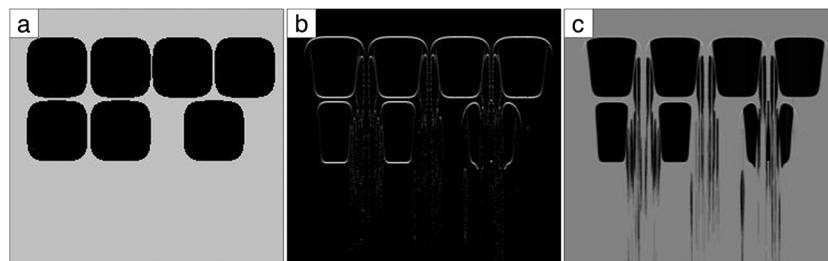


**Fig. 9** Illustration of refraction effects that limit analysis to single layer of air-filled alveoli. (a) Original alveolar shapes input into ray-tracing model. (b) Outlines of alveolar shapes calculated by ray-tracing model. (c) Resultant simulated OCT image.

shows a simulated image of two layers of alveoli created by the ray-tracing model with the refractive indices for fixed tissue and air. Whereas the first layer reconstructs as expected, the second layer of alveoli appears extremely distorted and would require complex correction to provide meaningful results.

However, any first layer of alveoli could potentially be imaged and analyzed deeper in the lung parenchyma through endoscopic or needle probes.<sup>9,23</sup> Because these more internal alveoli are not limited in their expansion by the pleura, they could have a significantly different shape compared to the alveoli analyzed within this study.

## 5 Conclusions

In this paper we present, to the best of our knowledge, the first validation of subpleural air-filled alveolar size measurements (cross-sectional area, perimeter, volume, and surface area) from OCT images. OCT underestimated alveolar sizes compared to measurements in micro-CT, but the relative changes were accurately represented. We have measured the group refractive index of fixed ( $n = 1.53$ ) and fresh ( $n = 1.41$ ) swine lung tissue at  $1310 \pm 55$  nm and confirmed the experimentally observed quantitative difference in alveolar sizes

between OCT and micro-CT images with a ray-tracing model. We have also established that refraction is the primary cause for measurement error of alveolar size from OCT images and have used our model to derive Eqs. (6) and (8), which calculate correction factors to approximate absolute measurements of superellipse and circular alveoli, respectively.

Whereas we expect differences in the refraction effects between fixed and fresh tissue, the ray-tracing results indicate that the differences are proportional and OCT can be used to quantify alveolar size and mechanistic changes during various ventilation settings *in vivo*.

## Acknowledgments

The authors thank Elkan Halpern from the MGH Institute for Technology Assessment and Benoit Piednoir from Air Liquide for expert statistical advice, as well as Hao Wang and Veronica Delaney for help with the tissue paste preparation and with the index measurement. This work has been supported by Air Liquide R&D, Medical Gases, Les-Loges-en-Josas, France. Additional funds were provided by the Center for Biomedical OCT Research and Translation through grant number P41EB015903, awarded by the National Center for Research

Resources and the National Institute of Biomedical Imaging and Bioengineering of the National Institutes of Health.

## References

1. A. A. Rostami, "Computational modeling of aerosol deposition in respiratory tract: a review," *Inhal. Toxicol.* **21**(4), 262–290 (2009).
2. S. Yun et al., "High-speed optical frequency-domain imaging," *Opt. Express* **11**(22), 2953–2963 (2003).
3. R. Leitgeb, C. Hitzenberger, and A. Fercher, "Performance of Fourier domain vs. time domain optical coherence tomography," *Opt. Express* **11**(8), 889–894 (2003).
4. J. G. Fujimoto et al., "Optical biopsy and imaging using optical coherence tomography," *Nat. Med.* **1**(9), 970–972 (1995).
5. L. P. Hariri et al., "Volumetric optical frequency domain imaging of pulmonary pathology with precise correlation to histopathology," *Chest* (2012).
6. C. I. Unglert et al., "Evaluation of optical reflectance techniques for imaging of alveolar structure," *J. Biomed. Opt.* **17**(7), 071303 (2012).
7. S. Meissner et al., "Virtual four-dimensional imaging of lung parenchyma by optical coherence tomography in mice," *J. Biomed. Opt.* **15**(3), 036016 (2010).
8. S. Meissner et al., "Three-dimensional Fourier domain optical coherence tomography *in vivo* imaging of alveolar tissue in the intact thorax using the parietal pleura as a window," *J. Biomed. Opt.* **15**(1), 016030 (2010).
9. R. A. McLaughlin et al., "Static and dynamic imaging of alveoli using optical coherence tomography needle probes," *J. Appl. Physiol.* **113**(6), 967–974 (2012).
10. L. Kirsten et al., "Four-dimensional imaging of murine subpleural alveoli using high-speed optical coherence tomography," *J. Biophoton.* **1**–5 (2012).
11. S. Meissner, L. Knels, and E. Koch, "Improved three-dimensional Fourier domain optical coherence tomography by index matching in alveolar structures," *J. Biomed. Opt.* **14**(6), 064037 (2009).
12. A. Golabchi et al., "Refractive errors and corrections for OCT images in an inflated lung phantom," *Biomed. Opt. Express* **3**(5), 1101–1109 (2012).
13. J. Bickenbach et al., "Comparison of two *in vivo* microscopy techniques to visualize alveolar mechanics," *J. Clin. Monit. Comput.* **23**(5), 323–332 (2009).
14. S. Meissner et al., "Simultaneous three-dimensional optical coherence tomography and intravital microscopy for imaging subpleural pulmonary alveoli in isolated rabbit lungs," *J. Biomed. Opt.* **14**(5), 054020 (2009).
15. G. J. Tearney et al., "Determination of the refractive index of highly scattering human tissue by optical coherence tomography," *Opt. Lett.* **20**(21), 2258–2260 (1995).
16. E. Namati et al., "Large image microscope array for the compilation of multimodality whole organ image databases," *Anat. Rec. (Hoboken)* **290**(11), 1377–1387 (2007).
17. M. D. Abramoff, P. J. Magelhaes, and S. J. Ram, "Image Processing with ImageJ," *Biophoton. Int.* **11**(7), 36–42 (2004).
18. J. M. Bland and D. G. Altman, "Statistical methods for assessing agreement between two methods of clinical measurement," *Lancet* **327**(8476), 307–310 (1986).
19. G. M. Hale and M. R. Querry, "Optical constants of water in the 200-nm to 200-microm wavelength region," *Appl. Opt.* **12**(3), 555–563 (1973).
20. F. P. Bolin et al., "Refractive index of some mammalian tissues using a fiber optic cladding method," *Appl. Opt.* **28**(12), 2297–2303 (1989).
21. E. A. Genina, A. N. Bashkatov, and V. V. Tuchin, "Tissue optical immersion clearing," *Expert Rev. Med. Devices* **7**(6), 825–842 (2010).
22. C. Schnabel et al., "Quantitative investigation of alveolar structures with OCT using total liquid ventilation during mechanical ventilation," *Proc. SPIE* **8207**, 82073A (2012).
23. B. C. Quirk et al., "In situ imaging of lung alveoli with an optical coherence tomography needle probe," *J. Biomed. Opt.* **16**(3), 036009 (2011).